
Beyond Accuracy and Alignment: A Diagnostic Evaluation Protocol for Feedback Alignment

Anonymous Author(s)

Affiliation

Address

email

Abstract

1 Modern feedback-alignment evaluation on deep residual networks is still summar-
2 ized by a deceptively simple pair: headline accuracy and headline cosine align-
3 ment Γ to the backpropagation gradient. We show that this pair can silently fail in
4 two distinct ways on standard CIFAR-10 pre-LayerNorm ResMLP and ViT-Mini
5 settings: first, *measurement degeneracy*, where residual-stream growth drives
6 hidden-layer BP gradients to the numerical floor and makes Γ uninterpretable;
7 and second, *low intrinsic credit-direction quality*, where random-feedback credit
8 remains essentially unaligned with BP on the deep blocks even when the reference
9 gradient is still meaningful. The headline result is that the field-standard reporting
10 pair walks back none of the methods we audit, whereas a four-diagnostic proto-
11 col walks back the three degenerate methods and passes the two trustworthy con-
12 trols. Intervention with a per-block scale-control penalty further reveals method-
13 dependent severity within the audited fixed-feedback family: State Bridge then
14 exceeds the architecture-matched frozen-blocks baseline by about 10 percentage
15 points, while Credit Bridge attains much higher deep BP cosine than DFA at the
16 same final accuracy, a dissociation that motivates reporting layerwise credit quality
17 jointly with a depth-utilization baseline. Our contribution is an evaluation method-
18 ology paper for the NeurIPS 2026 Evaluations & Datasets track: we provide the
19 protocol, the calibration logic for its thresholds, a reference implementation, a five-
20 method audit, and validation through temporal replay, cross-architecture checks,
21 intervention-based disambiguation, and a documented catalog of pipeline pitfalls,
22 in the spirit of critical evaluation analyses such as Jordan et al. [3], O’Bray et al.
23 [2], Paleka et al. [1].

24 1 Introduction

25 Feedback-alignment papers are usually judged by two numbers: task accuracy and an aggregate
26 similarity between the method’s local credit signal and the backpropagation gradient [4–7]. On
27 the audited 4-block $d=256$ ResMLP, however, Table 1 already shows that this pair is not a validity
28 check: DFA reaches only 0.306 ± 0.006 test accuracy, below the architecture-matched frozen-blocks
29 baseline of 0.349 ± 0.002 , while still looking superficially comparable to other non-BP methods.
30 Figure 1 further shows that the apparent cosine evidence is concentrated at the shallowest block,
31 with DFA at seed 42 reaching about $+0.42$ at layer 0 but approximately -0.03 to 0 on layers 1–4, so
32 the aggregate obscures where credit direction is and is not present. At the same time, the deepest BP
33 reference norm is only about 5×10^{-10} for DFA, State Bridge, and Credit Bridge, below the 10^{-8}
34 clamp used by `F.cosine_similarity`, whereas BP remains around 4×10^{-4} , so the reported deep
35 cosine is partly computed against a numerical-floor reference rather than an informative gradient

Table 1: Main audit table for the 4-block $d=256$ pre-LayerNorm ResMLP on CIFAR-10. The row and column structure is fixed here; fill from the three-seed audit output.

Method	Test acc.	Headline Γ	Status-quo verdict	Protocol verdict
BP	0.615 ± 0.003	≈ 1.0	trustworthy	trustworthy
EP	0.316 ± 0.030	0.008	trustworthy	trustworthy
DFA	0.306 ± 0.006	0.10	trustworthy	walked back
State Bridge	0.205 ± 0.032	0.005	trustworthy	walked back
Credit Bridge	0.289 ± 0.026	0.07	trustworthy	walked back

36 direction (Figure 1; Table 1). Those numbers can be useful, but only if the measurement regime
 37 itself is valid.

38 Our audit shows that modern residual vision models can make these two quantities look informative
 39 while failing to answer the question they are taken to answer. Figure 1 shows the first failure mode,
 40 which we call *Mode 1: measurement degeneracy*, where residual-stream growth drives the deepest
 41 hidden state to about $\|h_L\| \sim 10^8$ under DFA/SB/CB while the corresponding BP reference col-
 42 lapses to $\|g_L\| \sim 5 \times 10^{-10}$, so the deep-layer cosine is measured against a clamp-dominated floor
 43 rather than a meaningful target direction. The same figure also shows the second failure mode, *Mode*
 44 *2: low intrinsic credit-direction quality*, because even after comparing against the stronger frozen-
 45 blocks baseline (0.349 ± 0.002) and looking layer-by-layer, DFA’s deep blocks remain essentially
 46 null while only layer 0 is visibly positive. Intervention sharpens both modes. Adding a per-block
 47 residual penalty $\lambda \|f_i(h_i)\|^2$ to DFA at $\lambda=10^{-2}$ contains $\|h_L\|$ to about 4×10^4 and lifts the deep BP
 48 reference to about 10^{-6} , but DFA’s rescued deep cosine is only about $+0.16$; State Bridge under the
 49 same intervention reaches a three-seed deep cosine of $+0.32$ and, unlike DFA, exceeds the frozen-
 50 blocks baseline by $+10$ points in final accuracy; Credit Bridge reaches a deep cosine near $+0.68$
 51 yet matches only the DFA accuracy, so Mode 2 has method-dependent severity and deep cosine is
 52 not a sufficient predictor of final accuracy across methods. At the same time, at $\lambda=10^{-4}$ Mode 1 is
 53 alleviated while the DFA deep cosine still stays near zero, and at vanilla DFA epoch 1 the reference
 54 is already meaningful at about 6×10^{-7} but the deep cosine is still -0.008 ± 0.013 across three
 55 seeds. The failure is therefore neither unitary nor uniform: Mode 1 and Mode 2 are observationally
 56 separable, and within the audited fixed-feedback family, the severity of each mode varies by method.

57 Accordingly, this paper does not introduce a new FA variant or a new benchmark. Instead, Table 1
 58 and Figure 1 use a standard five-method CIFAR-10 audit to show that status-quo reporting would
 59 treat BP, EP, DFA, State Bridge, and Credit Bridge as the same kind of evidence-bearing object
 60 even though only BP and EP remain trustworthy under matched diagnostic checks. This makes the
 61 contribution methodological in the sense of Jordan et al. [3], O’Bray et al. [2], and Paleka et al. [1]:
 62 the central question is not whether one more FA variant can post a headline number, but whether the
 63 reporting pipeline distinguishes meaningful credit-direction evidence from numerical-floor artifacts
 64 and from shallow-only learning. The protocol therefore starts from per-layer diagnostics and a
 65 frozen-blocks baseline before reading any aggregate cosine or final accuracy as evidence about deep
 66 credit assignment. We first show the walk-back on a standard audit, then isolate the two failure
 67 modes, and finally state the reporting protocol that future FA papers should satisfy.

68 2 Audit: Standard Reporting Walks Back Nothing

69 We begin with the smallest setting in which all methods can be compared head-to-head under iden-
 70 tical architecture, optimizer family, and data. Table 1 fixes that canonical audit to a 4-block pre-
 71 LayerNorm ResMLP with width $d=256$ on CIFAR-10, trained for 100 epochs with AdamW (learn-
 72 ing rate 10^{-3} , weight decay 0.01), a cosine schedule, and three seeds (42, 123, 456). Within that
 73 single setting, BP, EP, DFA, State Bridge, and Credit Bridge can be read against the same architec-
 74 ture and the same training budget, while Figure 1 summarizes the corresponding per-block growth,
 75 deepest-layer BP reference norm, cross-batch stability, and frozen-baseline comparison. This is the
 76 table a reader would normally use to decide whether the methods trained the deep network.

77 By the field’s usual criteria, the non-BP methods appear to train to nontrivial accuracy and report
 78 nonzero alignment. In Table 1, DFA reaches 0.306 ± 0.006 test accuracy with headline $\Gamma=0.10$,
 79 State Bridge reaches 0.205 ± 0.032 with $\Gamma=0.005$, and Credit Bridge reaches 0.289 ± 0.026 with

5-method audit on 4-block $d=256$ ResMLP CIFAR-10 (3-seed mean \pm std)

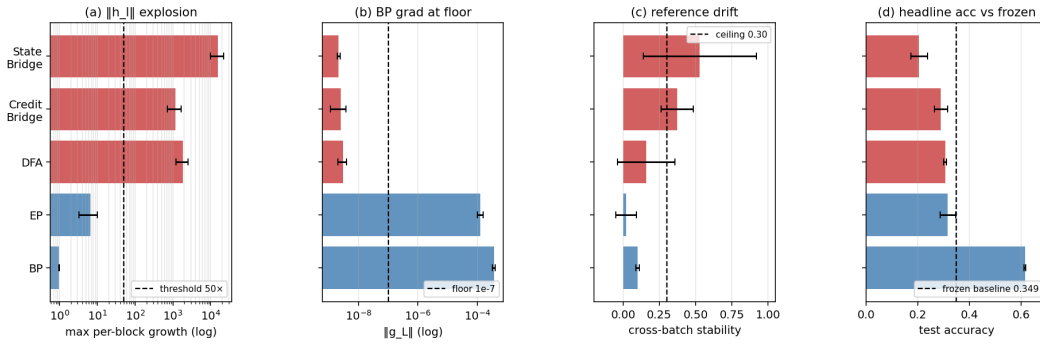


Figure 1: Five-method audit on the 4-block $d=256$ pre-LayerNorm ResMLP: the field-standard pair looks superficially consistent across methods, but the diagnostic view separates trustworthy controls from walked-back methods.

80 $\Gamma=0.07$; none of these rows looks like an obvious invalidation if one is reading the usual pair of final
 81 accuracy and aggregate alignment in the style of prior FA reporting [4–7]. Even the absolute scale
 82 does not itself force a walk-back, because all three methods are plainly above chance and all three
 83 report positive headline alignment rather than a visibly broken or undefined quantity. That reading
 84 is exactly what the rest of the paper overturns.

85 Low accuracy by itself is not the pathology. EP is the key internal comparison in Table 1 and
 86 Figure 1: it achieves only 0.316 ± 0.030 accuracy and a very small headline $\Gamma=0.008$, yet its per-
 87 block growth is only $11.6\times$, its deepest BP reference norm remains around 1.3×10^{-4} rather than
 88 collapsing to the numerical floor, and its cross-batch direction-stability score is 0.02 rather than the
 89 much higher drift-dominated values seen for DFA-family methods. At the same time, EP is not a
 90 positive result for depth usage in the stronger sense, because its trainable-model accuracy is still
 91 3.3 percentage points below the frozen-blocks baseline of 0.349 ± 0.002 . The distinction matters
 92 because it separates underperformance from invalid evaluation.

93 When we compare each method to a frozen-blocks baseline matched to the same architecture, the
 94 headline interpretation changes immediately. The frozen-blocks model, which trains only the em-
 95 bedding, LayerNorm, and head while holding the residual blocks fixed, reaches 0.349 ± 0.002 across
 96 the same three seeds; against that baseline, BP is higher by 26.6 points, but DFA is lower by 4.3
 97 points, State Bridge by 14.4 points, Credit Bridge by 6.0 points, and even EP by 3.3 points. Fig-
 98 ure 1 shows that this accuracy comparison lines up with the diagnostic split: DFA, State Bridge, and
 99 Credit Bridge also combine extreme per-block growth ($237\times$, $12000\times$, and $96\times$), deepest-layer BP
 100 norms around 10^{-9} , and high cross-batch instability (0.16, 0.53, and 0.37), so their deep blocks are
 101 at best passengers and in practice often harmful. This establishes the audit question the rest of the
 102 paper must answer: why do the standard signals fail so badly?

103 3 Failure Mode 1: Measurement Degeneracy

104 Mode 1 has two parts. The activation-growth part (a) is a scale pathology of fixed-feedback local-
 105 credit objectives without an effective scale-control term: for block l , DFA, State Bridge, and Credit
 106 Bridge each update f_l by reducing a local loss of the form $-\langle f_l(h_l), a_l \rangle$, where the per-layer credit
 107 vector a_l is the method-specific projection of the output error (for DFA, $a_l = B_l^\top e_T$ with a fixed
 108 random B_l ; for State Bridge, a_l is the gradient of a cross-entropy loss measured through a learned
 109 state predictor $G_\psi(h_l, t_l, s)$ that estimates h_L ; for Credit Bridge, a_l is the gradient of a learned
 110 value network $V(h_l, t_l, s)$). None of these three local losses contains a penalty on $\|f_l(h_l)\|$, so any
 111 direction in which a larger block output improves inner-product alignment with the method’s fixed
 112 or learned credit target is rewarded; in a pre-LN residual stack, larger block outputs directly increase
 113 residual-stream scale, and terminal LayerNorm at the output removes task-loss sensitivity to that
 114 scale, so the architecture supplies no global restraint on the local growth incentive. The gradient-
 115 floor part (b) follows from the LayerNorm Jacobian: in terminal-LN architectures $\partial \text{LN}(h)/\partial h \propto$
 116 $1/\|h\|$ in expectation, so the same residual-stream inflation is accompanied by collapse of the hidden-

117 layer BP reference norm. Empirically, on the audited 4-block pre-LayerNorm ResMLP ($d=256$,
 118 CIFAR-10, 100 epochs, 3 seeds), DFA training drives $\|h_L\|$ from about 9 at initialization to about
 119 4×10^8 by epoch 100 and $\|g_L\|$ from about 9.8×10^{-4} to about 5×10^{-10} , while the reported deep
 120 cosine remains defined only because `F.cosine_similarity` clamps the denominator at $\varepsilon=10^{-8}$
 121 (Table 1; Figure 1). At that endpoint the reference norm is about $20\times$ below the clamp, so the
 122 quantity being reported is effectively $(a \cdot b)/(\|a\| \max(\|b\|, 10^{-8}))$ rather than a comparison to a
 123 meaningful BP direction.

124 We tested this mechanism story against four natural alternative attributions, all of which it survives.
 125 *Not residual-skip-driven*: on the same ResMLP-d256 with terminal LN kept and the additive skip
 126 removed ($h_{l+1}=F_l(h_l)$), DFA still inflates $\|h_L\|$ from ~ 5 to $\sim 2.2 \times 10^4$ in three epochs and con-
 127 verges to $\|h_L\| \approx 1.06 \times 10^8$ and $\|g_L\| \approx 1.09 \times 10^{-10}$ at 100 epochs, both already at the diagnostic
 128 floor (Appendix H). *Not task-signal-driven*: replacing labels by i.i.d. random class targets refreshed
 129 every minibatch on the same backbone, DFA still reaches $\|h_L\| \approx 1.67 \times 10^8$ and $\|g_L\| \approx 8 \times 10^{-12}$ at
 130 100 epochs while accuracy stays at chance (Appendix I). *Not DFA-specific*: the same random-target
 131 ablation also drives $\|h_L\|$ from 9 to 6.2×10^3 for State Bridge and 2.0×10^4 for Credit Bridge in three
 132 epochs, again at chance accuracy, so all three audited fixed-feedback methods exhibit data-agnostic
 133 activation growth (Appendix I). *Not shared by EP*: under the same random-target protocol, EP keeps
 134 $\|h_L\| \approx 586$ at five epochs of training, $25\times$ smaller than DFA’s three-epoch value on the same archi-
 135 tecture, consistent with EP’s bounded behavior on real labels and confirming that the random-target
 136 assay separates the explosion-prone fixed-feedback class from EP’s energy-based local objective.

137 The matched same-backbone causal control for diagnostic (b) is removing terminal LayerNorm. On
 138 the same ResMLP-d256 with the residual skip intact, 100 epochs of DFA, three seeds, the residual
 139 stream still inflates to $\|h_L\| \approx 1.21 \times 10^7$, but the deepest hidden-layer BP gradient remains at
 140 $\|g_L\| \approx 7.2 \times 10^{-4}$ (four orders of magnitude above the diagnostic (b) floor), and the final test
 141 accuracy is 0.327 ± 0.012 , statistically indistinguishable from vanilla DFA’s 0.306 ± 0.006 on the
 142 same backbone with terminal LayerNorm intact. Removing terminal LayerNorm therefore preserves
 143 Mode 1 (a) but cleanly eliminates Mode 1 (b) on the same architecture, while leaving final task
 144 accuracy essentially unchanged. Combined with the broader cross-architecture pattern (StudentNet
 145 and the BatchNorm CNN, which lack terminal LayerNorm, never trigger diagnostic (b); ViT-Mini
 146 with a terminal LN does, by epochs 2–3 (Figure 2)), terminal LayerNorm is necessary for Mode 1 (b)
 147 in the audited residual ResMLP and ViT-Mini setting. The collapse is also not a late-epoch curiosity:
 148 $\|g_L\|$ drops from 9.8×10^{-4} at epoch 0 to 6.7×10^{-8} by epoch 4 in the temporal replay across three
 149 seeds, so the protocol fires within the first 11 epochs of a 100-epoch run and is actionable as an
 150 early-stop criterion rather than a post hoc explanation. Once measurement degeneracy is identified,
 151 the next question is whether poor deep credit remains even before collapse.

152 4 Failure Mode 2: Low Intrinsic Credit-Direction Quality

153 The second failure mode appears even in the meaningful-measurement regime. At the earliest vanilla
 154 DFA checkpoints on ResMLP, the hidden backpropagated gradient at the first deep block remains
 155 above the numerical floor: at epoch 1, $\|g_2\|$ is 6.7×10^{-7} , 6.5×10^{-7} , and 3.9×10^{-7} across the three
 156 seeds, all above the 10^{-7} threshold used to distinguish measurable from collapsed gradients. Yet the
 157 corresponding deep-layer cosine values are already essentially null: across layers 1–4, all seed-level
 158 measurements at epoch 1 lie in $[-0.04, +0.02]$, with a three-seed mean of -0.008 ± 0.013 , and by
 159 epoch 2 the deep mean is still only -0.018 ± 0.018 (Table 2). This is the observational pattern pre-
 160 dicted by low credit-direction quality rather than mere disappearance of signal: the gradient is still
 161 present enough to measure, but the directions delivered to the deep network carry little agreement
 162 with backpropagation, consistent with prior concerns that alternative feedback rules can fail by sup-
 163 plying poor credit assignments even before full collapse [8, 9, 11, 10]. This rules out the simplest
 164 objection that the deep-layer null result is merely a byproduct of collapse.

165 A second metric with different numerical failure modes tells the same story. Cosine measures di-
 166 rectional agreement with the BP gradient, whereas perturbation correlation ρ measures whether the
 167 proposed update predicts the correct sign and relative magnitude of loss change under actual per-
 168 turbations; their failure modes are therefore different, especially with respect to normalization and
 169 small-denominator effects. In our controls, ρ behaves as expected, with a Taylor-ceiling positive
 170 control near $+0.997$ and a random-vector negative control near $+0.006$ (Figure 3, Table 2). On
 171 vanilla DFA, deep ρ is likewise null: for the early checkpoints where the gradients remain measur-

172 able, the deep average is -0.003 ± 0.005 across seeds and epochs, and in a floor-level checkpoint it is
 173 $+0.002$, again indistinguishable from noise. The agreement between cosine and ρ therefore rules out
 174 the interpretation that the null deep result is an artifact of cosine’s ε -clamp or vector normalization.
 175 The deep blocks are not just hard to measure; they are receiving weakly useful directions.

176 Per-layer reporting is therefore not cosmetic. In ResMLP under vanilla DFA, the headline aggregate
 177 alignment $\Gamma \approx 0.07$ – 0.10 can look mildly positive only because layer 0 remains strongly aligned
 178 while the deep network is not: at the same early checkpoints where layers 1–4 are essentially zero,
 179 layer 0 has cosine $+0.42$, $+0.45$, and $+0.39$ across seeds (Table 2). The resulting average can there-
 180 fore be driven by the embedding layer even when the interior blocks are effectively unaligned, so
 181 aggregate reporting obscures the very distinction needed to separate “measurement collapse” from
 182 “poor credit direction.” This layer-0 dominance is specific to the ResMLP DFA setting; on ViT-Mini
 183 DFA, all layers are near zero, which strengthens the broader methodological point that alignment
 184 should be reported per layer rather than only in aggregate. With the two modes separated observa-
 185 tionally, the remaining question is whether intervention can move them independently.

186 Mode 2 has method-dependent severity within the audited fixed-feedback family once Mode 1 is
 187 alleviated. Applying the same per-block scale-control penalty $\lambda=10^{-2}$ that rescued DFA to State
 188 Bridge and to Credit Bridge on the same 4-block $d=256$ ResMLP backbone over 30 epochs and three
 189 seeds gives converged test accuracies of 0.453 ± 0.003 (SB) and 0.360 ± 0.003 (CB), with deep mean
 190 cosines of $+0.322 \pm 0.007$ (SB) and $+0.679 \pm 0.008$ (CB) and deep mean ρ of $+0.402 \pm 0.015$
 191 (SB) and $+0.464 \pm 0.025$ (CB), while DFA under the same intervention reaches 0.363 ± 0.001
 192 with deep cosine $+0.155 \pm 0.025$ and deep ρ $+0.080 \pm 0.011$ (Table 2; Appendix J). The State
 193 Bridge penalty rescue is roughly 24 percentage points above the vanilla State Bridge baseline of
 194 0.213 on the same architecture and, more importantly for the paper’s central walk-back, exceeds
 195 the architecture-matched frozen-blocks shallow baseline of 0.349 by $+10.4$ percentage points. State
 196 Bridge with the penalty intervention is therefore the first audited non-BP method whose trained deep
 197 blocks substantively improve over an architecture-matched random-block baseline; the headline accu-
 198 racy gap is comparable to BP+penalty’s $+18.1$ pp over the same shallow baseline. Neither the
 199 activation scale nor the deep BP gradient magnitude is silenced under the penalty: $\|h_L\|$ stays at
 200 302 ± 8 for SB and 5680 ± 178 for CB, with $\|g_L\|$ at $\sim 1.8 \times 10^{-4}$ and $\sim 1.9 \times 10^{-5}$ respectively,
 201 both well within the meaningful-measurement regime, so the recovered deep cosines are computed
 202 against an informative reference and not against a numerical floor. Within this rescued regime, the
 203 three methods reveal a clean cosine-versus-accuracy dissociation. Credit Bridge achieves roughly
 204 $4\times$ the deep cosine of DFA and $2\times$ that of State Bridge, yet its final accuracy matches DFA’s and
 205 is 9 percentage points below State Bridge’s. We therefore frame the Mode 2 reading as a three-part
 206 proposition. *Observation:* under the same intervention and matched training budget, CB and DFA
 207 reach the same accuracy despite a $4\times$ deep-cosine gap, while SB is the best accuracy with interme-
 208 diate cosine. *Inference:* layerwise cosine to the BP gradient is necessary to rule out grossly wrong
 209 credit signals (it distinguishes the rescued regime from the clamp-dominated vanilla regime), but
 210 it is not sufficient to certify that the supplied signal is useful credit for depth. *Mechanism hypoth-*
 211 *esis:* usefulness depends on whether the local update induces useful forward-state change across
 212 blocks, not merely whether its direction is close to the BP gradient in angle. Under this reading, CB
 213 supplies a gradient-direction surrogate that aligns with BP in angle but does not translate to a coordi-
 214 nated forward-state improvement, while State Bridge supplies a state-level downstream teaching
 215 signal that preserves aspects of useful credit which layerwise cosine does not measure. We state this
 216 as a mechanism hypothesis rather than a theorem because we have measured the angle-to-accuracy
 217 gap but not the full functional-credit content; the reporting rule that follows is robust to either inter-
 218 pretation. This cross-method dissociation strengthens the methodological point that alignment must
 219 be reported jointly with measurement validity and a depth-utilization baseline rather than as a single
 220 headline number.

221 5 Intervention and Cross-Architecture Evidence

222 The penalty intervention first matters as a rescue of the measurement regime. When we add a per-
 223 block penalty $\lambda \text{mean}(\|f_i(h_i)\|^2)$ to DFA’s local loss and train the 4-block $d=256$ ResMLP for 30
 224 epochs on CIFAR-10, the $\lambda=10^{-2}$ setting contains the terminal hidden-state scale from $\|h_L\| \sim$
 225 4.4×10^8 under vanilla DFA to $\sim 4.0 \times 10^4$, while lifting the deepest BP reference norm from
 226 $\|g_L\| \sim 5 \times 10^{-10}$ to $\sim 9.0 \times 10^{-7}$, a roughly four-order-of-magnitude rescue on both quantities

Table 2: Two-mode validation table built around the intervention and disambiguation results.

Condition	Deep-layer alignment signal	Measurement regime	Interpretation
Vanilla DFA, early epoch	$\overline{\text{cos}}_{deep} = -0.008 \pm 0.013, \overline{\rho}_{deep} = -0.003 \pm 0.005$	meaningful ($\ g\ \sim 10^{-6}$)	mode 2 present without m
Vanilla DFA, converged	$\overline{\text{cos}}_{deep} = -0.022, \overline{\rho}_{deep} = +0.002$	degenerate ($\ g\ \sim 10^{-9}$)	mode 1 obscures mod
Penalized DFA, $\lambda=10^{-2}$	$\overline{\text{cos}}_{deep} = +0.155 \pm 0.025, \overline{\rho}_{deep} = +0.080 \pm 0.011$	meaningful ($\ g\ \sim 10^{-6}$)	partial alleviation of both
Fresh- B null control	$\overline{\text{cos}}_{deep} = +0.002 \pm 0.022$ ($n=20$ draws)	meaningful	training-specific adaptation

227 (Figure 3; Table 2). At that setting, both diagnostic (a) and diagnostic (b) pass on penalized DFA,
 228 and test accuracy rises to 0.363 ± 0.001 from 0.308 ± 0.014 for vanilla DFA. The key point is not
 229 yet that the recovered network has good deep credit, but that the deep reference vector is again large
 230 enough to function as a meaningful target direction rather than a clamp-dominated artifact. That
 231 rescue makes the second question measurable rather than hypothetical.

232 Once the reference vector is meaningful again, the deep layers no longer sit exactly at null. At
 233 $\lambda=10^{-2}$, penalized DFA reaches a three-seed deep-layer mean cosine of $+0.155 \pm 0.025$ and deep
 234 perturbation correlation of $+0.080 \pm 0.011$, whereas vanilla DFA is essentially zero on both metrics
 235 in the deep blocks, consistent with prior concerns that alternative feedback can fail by supplying
 236 poor credit directions even before full collapse [8, 9, 11, 10]. The null calibration rules out the inter-
 237 pretation that this recovered signal is merely measurement noise: on the same penalized checkpoint,
 238 replacing the training-time feedback matrices with 20 fresh random B_i draws gives a deep cosine
 239 of only $+0.002 \pm 0.022$, with per-layer standard deviations of 0.013–0.023, all within noise of zero
 240 (Table 2). The λ sweep sharpens the dissociation further: at $\lambda=10^{-4}$, Mode 1 is already alleviated,
 241 with $\|h_L\|=2.4 \times 10^4$ and $\|g_L\|=6.3 \times 10^{-7}$, but deep cosine remains -0.022 , while at $\lambda=10^{-2}$ it
 242 rises to $+0.165$ and deep ρ to $+0.091$ (Figure 3). The improvement is real, but it is only partial.

243 A rescue intervention is only informative if its direct cost is controlled. The relevant control is BP
 244 trained under the same penalty: BP falls from 0.609 ± 0.004 without the penalty to 0.530 with
 245 $\lambda=10^{-2}$, so the penalty has a direct cost of about 8 percentage points even when credit assignment
 246 is correct, whereas DFA moves in the opposite direction, from 0.308 ± 0.014 to 0.363 ± 0.001 ,
 247 and State Bridge moves further still, from 0.213 to 0.453 ± 0.003 (three seeds), under the same
 248 intervention (Figure 3; Appendix J). Relative to the frozen-blocks baseline of 0.349 , BP+penalty
 249 retains a margin of $+18.1$ points, State Bridge+penalty retains $+10.4$ points, and DFA+penalty
 250 retains only $+1.4$ points. The remaining BP-to-DFA gap of 17 points is therefore a lower bound
 251 on the part of DFA’s deficit that is not explained by simple penalty-induced capacity loss alone,
 252 though not a clean isolation because BP uses an end-to-end loss whereas DFA uses block-local
 253 losses. The substantially smaller BP-to-State-Bridge gap of $0.530 - 0.453 = 7.7$ points shows
 254 that the cross-method differences in penalty-rescued accuracy are not all attributable to a uniform
 255 “random-feedback ceiling”: the bridge construction in State Bridge can recover much more of the
 256 BP-with-penalty performance than DFA can, on the same architecture and the same intervention.
 257 The residual gap after that control is what keeps Mode 2 substantively alive while letting it have
 258 method-dependent severity.

259 The architecture comparison sharpens the scope of the critique. In the terminal-LN architectures we
 260 audited, both diagnostics fire for DFA-trained ResMLP at $d=256$, the same pattern recurs at $d=512$
 261 with even larger max-per-block growth (about 1.5×10^4), and ViT-Mini with a class token and termi-
 262 nal LN shows diagnostic (a) by epoch 1 and diagnostic (b) by epochs 2–3 (Figure 2). A depth
 263 sweep on the $d=512$ ResMLP at $L \in \{2, 4, 6, 8, 12\}$ shows that the layerwise pattern is essentially
 264 depth-invariant: DFA’s layer-0 cosine stays in $[+0.39, +0.40]$ across all five depths, while its mean
 265 deep-layer cosine stays within $[-0.005, +0.000]$ and its deep perturbation correlation collapses to
 266 0.000 in every depth tested, even though BP retains a deep-layer cosine of $+0.94$ at $L=12$ (Ap-
 267 pendix G). The deep credit signal does not improve when the network is shallower, so the failure
 268 is not a “too deep” artifact. In the non-terminal-LN controls, the pattern is different: StudentNet
 269 shows diagnostic (a) only at epochs 14–25 while diagnostic (b) never fires across 100 epochs and
 270 three seeds, and the BatchNorm CNN on CIFAR-10 likewise shows strong growth under DFA, with
 271 max-per-block growth up to $237\times$, but keeps deepest BP gradients around $\|g\| \sim 10^{-3}$ and never
 272 triggers diagnostic (b) (Figure 2). BP never triggers either diagnostic in any audited architecture.
 273 The matched same-backbone ResMLP-d256 ablation in Section 3 supplies the cleanest causal control:
 274 removing terminal LayerNorm from the same architecture preserves activation growth but elim-

Cross-architecture temporal evolution of FA diagnostics (seed 42)

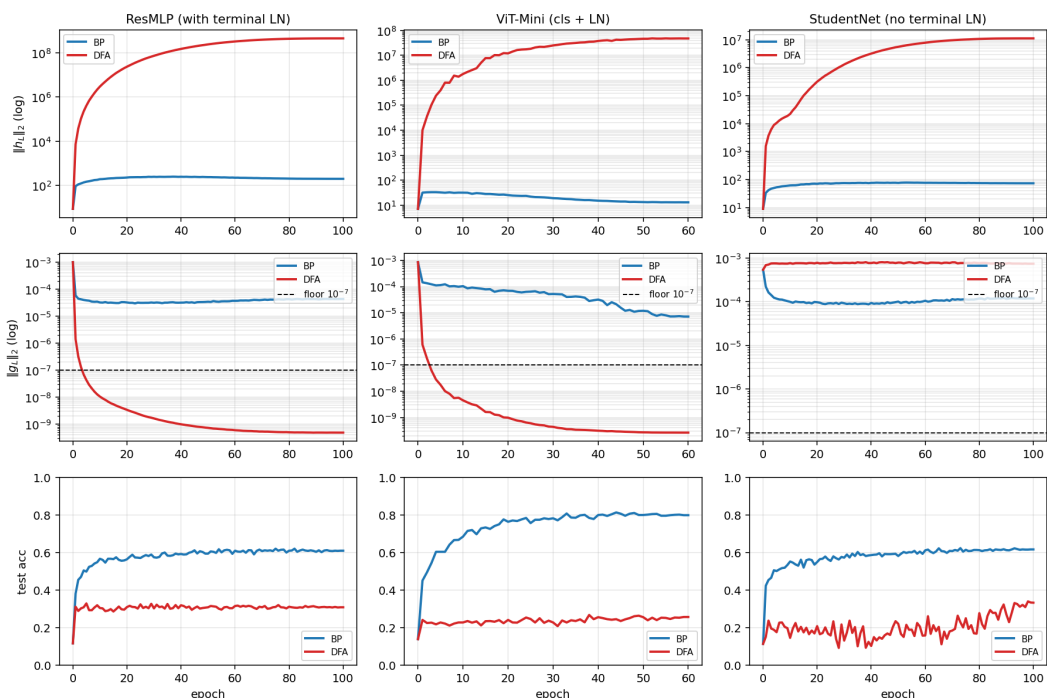


Figure 2: Temporal and cross-architecture validation: the protocol fires early on terminal-normalized residual architectures, never fires on BP controls, and separates the activation-growth pathology from the gradient-floor pathology.

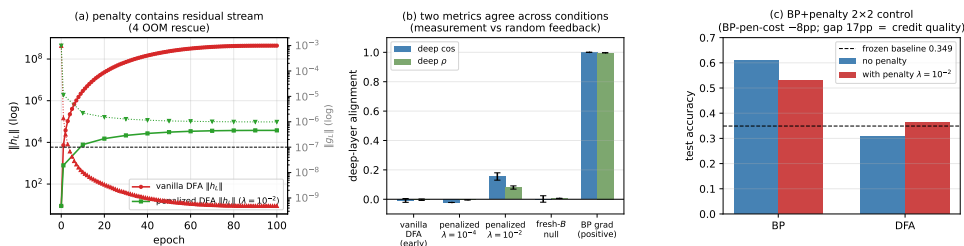


Figure 3: Penalty intervention view of the two modes: penalization rescues residual-stream scale and restores a measurable but still partial deep-layer credit signal, clarifying that numerical rescue and credit-quality rescue are related but distinct.

275 inates the gradient floor, so diagnostic (b) is necessary on terminal-LN ResMLP and is not just an
 276 architecture-class coincidence. The broader claim therefore holds at full strength inside the audited
 277 residual ResMLP and ViT-Mini regime, while diagnostic (a) remains useful more broadly. This lets
 278 the paper end with a reporting rule rather than an overclaimed theory.

279 6 Recommended FA Evaluation Protocol

280 The reporting protocol begins with measurement validity. Before any FA paper reports a headline
 281 alignment number, it should report per-layer state scale and the hidden BP reference-gradient scale
 282 at the layers where the scientific claim is being made. In our audited regime, those two quantities
 283 already separate healthy from invalid measurement with unusually wide margins: the maximum
 284 per-block growth stays below about $11\times$ for BP and EP but is at least $694\times$ for the degenerate
 285 methods, giving a $63\times$ calibration gap, while the deepest hidden BP norm stays above about 10^{-4}
 286 for BP and EP but below about 4×10^{-9} for the degenerate methods, giving a $24,338\times$ gap (Table 3;

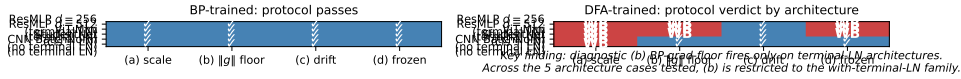


Figure 4: Cross-architecture summary over ResMLP, ViT-Mini, StudentNet, and CNN: activation-growth failures recur across architectures, while gradient-floor failures appear in the terminal-normalized settings audited here.

Table 3: Protocol definition table. Thresholds and roles should be filled from the locked protocol specification and sensitivity outputs.

Diag.	Measurement	Default threshold	Role
(a)	Per-layer activation scale via max-per-block growth $\max_l \ h_{l+1}\ /\ h_l\ $	$> 50\times$	binary detector
(b)	Deepest hidden-layer BP gradient norm $\ g_L\ $	$< 10^{-7}$	binary detector
(c)	Cross-batch direction stability of normalized BP gradients	> 0.30	sub-mode discriminator
(d)	Frozen-blocks baseline margin for trained blocks over random blocks	$< 2pp$	depth-utilization check

287 Table 1; Figure 4). These are not cosmetic diagnostics around the real result: they determine whether
 288 the reported cosine is being computed against an informative BP direction or against a floor-level
 289 reference. If the reference gradient is at floor, the evaluator should stop treating aggregate alignment
 290 as evidence.

291 The point of the protocol is not to add plots; it is to prevent a specific class of false conclusions. For
 292 this paper, the minimal protocol is four checks: per-layer activation scale via max-per-block growth,
 293 deepest hidden BP gradient floor, meaningful-regime per-layer credit quality, and an architecture-
 294 matched frozen-blocks baseline (Table 3). The first two ask whether the reference quantity is still
 295 valid; the third asks whether, once validity is restored, the deep blocks receive useful directions;
 296 and the fourth asks whether the trained depth is doing better than a model whose residual blocks
 297 were never trained at all. Figure 5 makes the decision value explicit: accuracy alone walks back
 298 0/5 audited methods, accuracy plus headline Γ still walks back 0/5, and the full protocol walks
 299 back 3/5 by flagging DFA, State Bridge, and Credit Bridge, with diagnostics (a), (b), and (d) each
 300 independently sufficient for binary detection on those failures. On our audit, these checks catch
 301 failures that accuracy plus aggregate alignment miss completely.

302 A useful evaluation rule should reject the bad cases without collapsing everything into a negative
 303 result. The protocol is conservative in exactly that sense: it preserves BP and EP as evidence-bearing
 304 controls, and it walks back only those claims that fail measurement-validity or depth-utilization
 305 checks in Table 1. That asymmetry is important because the thresholds are not equally strong in
 306 the same way. Diagnostics (a) and (b) have sharp empirical calibration gaps in the audited regime,
 307 diagnostic (c) is explicitly a sub-mode discriminator rather than a primary detector, and diagnostic
 308 (d) uses a deliberately weak 2pp margin as a context check rather than a theorem about useful depth.
 309 The rule therefore does not say that low accuracy, low aggregate alignment, or any non-BP method is
 310 automatically invalid; it says only that claims unsupported by measurement-valid evidence should be
 311 withdrawn, while trustworthy controls should remain standing. The Section 4 cross-method cosine-
 312 versus-accuracy dissociation reinforces the necessity of keeping all four diagnostics separate: Credit
 313 Bridge, State Bridge, and DFA differ by more than a factor of four in deep-layer alignment under the
 314 same penalty rescue without tracking final accuracy in the same direction, so aligning an alternative
 315 credit rule with the BP gradient is not a substitute for checking depth utilization against a matched
 316 shallow baseline. That conservative asymmetry is why the protocol belongs in the main paper rather
 317 than the appendix.

318 7 Discussion, Limits, Conclusion

319 Our claim is about what existing evidence licenses, not about impossibility. This paper does not show
 320 that FA cannot work in deep networks; it shows that current evaluation practice can misread what
 321 happened by letting headline accuracy and aggregate alignment stand in for measurement validity

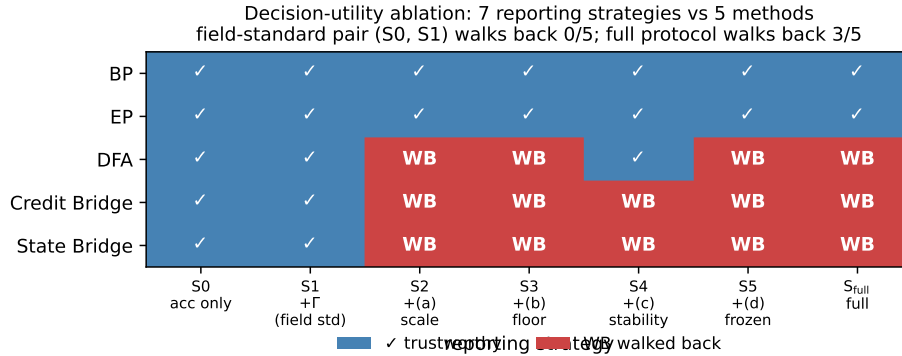


Figure 5: Decision-utility ablation comparing the field-standard reporting pair against progressively richer diagnostic strategies: accuracy only and accuracy+ Γ walk back no audited failures, while the full protocol walks back the three silent failures.

322 and layerwise credit quality. The strongest examples are precisely the cases where the field-standard
323 summary would sound mildly positive while the audited deep evidence has already collapsed or
324 is already null: DFA, State Bridge, and Credit Bridge all survive status-quo reporting in Table 1,
325 yet the protocol shows that their deep claims are unsupported. The intervention results in Figure 3
326 reinforce the same distinction, because restoring a measurable regime partially rescues deep credit
327 signal rather than proving that the original headline had been trustworthy all along. That distinction
328 is important because evaluation failure and algorithmic impossibility are different statements.

329 The right level of generality is the audited regime. Our strongest claim is scoped to modern resid-
330 ual vision architectures, especially the pre-LayerNorm and terminal-LayerNorm settings where we
331 directly observed Mode 1: the 4-block ResMLP at $d=256$, its $d=512$ extension, and ViT-Mini all
332 show the same basic pattern, whereas StudentNet and the BatchNorm CNN refine the scope by show-
333 ing that activation-growth failures can persist without the hidden-gradient-floor collapse (Figure 4;
334 Figure 3). That leaves clear limits. The dataset is only CIFAR-10, the models are small to medium
335 rather than frontier-scale, the terminal-LayerNorm-necessity claim for diagnostic (b) is established
336 causally on the audited residual ResMLP via the matched same-backbone no-terminal-LN control
337 but not proven to extend beyond that architecture family, and the BP-plus-penalty comparison is only
338 a lower-bound control on penalty cost rather than a perfect decomposition. Those limitations narrow
339 what is claimed, but they do not weaken the core methodological point that the audited measurement
340 regime can fail silently in exactly the architectures that now dominate this genre of experiment. Fu-
341 ture positive or negative examples outside this regime would refine the scope of the protocol, not
342 invalidate the critique.

343 The main lesson is to decompose the evaluation question before interpreting the answer. Future
344 FA papers should report, separately, whether the BP reference is still meaningful, whether the
345 deep layers receive useful credit in that meaningful regime, and whether trained depth beats an
346 architecture-matched frozen-blocks baseline, instead of compressing those distinct questions into a
347 single headline accuracy or headline Γ . That is the sense in which this paper fits the evaluation-
348 methodology line of Jordan et al. [3], O’Bray et al. [2], and Paleka et al. [1]: the contribution is not a
349 new benchmark artifact, but a reporting rule for preventing a repeatable interpretive error. Once the
350 field enforces that separation between measurement validity and substantive credit quality, positive
351 results will become more trustworthy and negative results more precise. Once that decomposition
352 is enforced, the apparent evidence for successful deep credit assignment becomes much harder to
353 overstate.

354 References

- 355 [1] Daniel Paleka et al. Pitfalls in evaluating language model forecasters. In *International Confer-*
356 *ence on Learning Representations*, 2026.
- 357 [2] Leslie O’Bray et al. Evaluation metrics for graph generative models: problems, pitfalls, and
358 practical solutions. In *International Conference on Learning Representations*, 2022.

- 359 [3] Scott M. Jordan et al. Evaluating the performance of reinforcement learning algorithms. In
360 *International Conference on Machine Learning*, 2020.
- 361 [4] Timothy P. Lillicrap, Daniel Cownden, Douglas B. Tweed, and Colin J. Akerman. Random
362 synaptic feedback weights support error backpropagation for deep learning. *Nature Communi-*
363 *cations*, 7:13276, 2016.
- 364 [5] Arild Nøkland. Direct feedback alignment provides learning in deep neural networks. In
365 *Advances in Neural Information Processing Systems*, 2016.
- 366 [6] Mohamad Akrouf, Collin Wilson, Peter C. Humphreys, Timothy P. Lillicrap, and Douglas B.
367 Tweed. Deep learning without weight transport. In *Advances in Neural Information Processing*
368 *Systems*, 2019.
- 369 [7] Julien Launay, Iacopo Poli, François Boniface, and Florent Krzakala. Direct feedback align-
370 ment scales to modern deep learning tasks and architectures. In *Advances in Neural Informa-*
371 *tion Processing Systems*, 2020.
- 372 [8] Sergey Bartunov, Adam Santoro, Blake A. Richards, Luke Marris, Geoffrey E. Hinton, and
373 Timothy P. Lillicrap. Assessing the scalability of biologically motivated deep learning algo-
374 rithms and architectures. In *Advances in Neural Information Processing Systems*, 2018.
- 375 [9] Theodore H. Moskovitz, Ashok Litwin-Kumar, and L. F. Abbott. Feedback alignment in deep
376 convolutional networks. *arXiv preprint arXiv:1812.06488*, 2018.
- 377 [10] Maria Refinetti, Stéphane d’Ascoli, Ruben Ohana, and Sebastian Goldt. Align, then memorise:
378 the dynamics of learning with feedback alignment. In *International Conference on Machine*
379 *Learning*, 2021.
- 380 [11] Brian Crafton, Abhinav Parihar, Evan Gebhardt, and Arijit Raychowdhury. Direct feedback
381 alignment with sparse connections for local learning. *Frontiers in Neuroscience*, 13:525, 2019.
- 382 [12] Ruibin Xiong, Yunchang Yu, et al. On layer normalization in the transformer architecture. In
383 *International Conference on Machine Learning*, 2020.

384 A Reference Implementation

385 We will release a reference implementation at [https://github.com/](https://github.com/REPO-URL-TO-BE-INSERTED)
386 `REPO-URL-TO-BE-INSERTED`. The release is intended to make the evaluation protocol easy
387 to run and difficult to misreport: it contains one command path for training or loading checkpoints,
388 one command path for computing the four diagnostics, and one command path for rendering the
389 audit tables and figures used in the paper. The reference code should be treated as part of the
390 evaluation artifact rather than as an auxiliary convenience, because several of the failure cases in
391 this paper arise from seemingly minor choices in how gradients, layers, and baselines are measured.

392 The repository is organized around the claims in the paper rather than around model classes. A min-
393 imal run should expose: (i) architecture-matched trainable-block and random-block baselines, (ii)
394 per-layer residual-scale and BP-gradient measurements at fixed checkpoints, (iii) deep-layer cosine
395 computations with the exact batch and masking conventions used by the audit, and (iv) summary
396 scripts that emit the tables underlying Table 1, Table 2, and Table 3. The goal is that an outside
397 reader can reproduce both the verdict and the reason for the verdict from a single checkpoint bundle
398 without reverse-engineering hidden notebook logic.

399 B Pipeline Pitfalls Catalog

400 **Pitfall 1: Layer-0 dominance hidden by global averaging.** A single global cosine can look
401 mildly positive even when all deep trainable blocks are effectively null, because the shallowest layer
402 dominates the norm budget. The protocol therefore treats layerwise inspection as mandatory and
403 interprets any aggregate headline only after checking where the signal comes from.

404 **Pitfall 2: Cosine against a numerical-floor BP reference.** If the deepest BP gradient norm has
405 collapsed, the cosine to that vector is not a trustworthy direction-quality measurement. This is the
406 core measurement-degeneracy failure, and it is why the protocol records $\|g_L\|$ before interpreting
407 any deep-layer alignment statistic.

408 **Pitfall 3: Batch mismatch between reference and candidate gradients.** Using different mini-
409 batches, different augmentations, or different dropout masks for BP and FA credit vectors can inflate
410 or destabilize the reported cosine. The reference implementation computes both vectors on the same
411 frozen forward pass whenever the claim being tested is directional agreement rather than training
412 robustness.

413 **Pitfall 4: Baseline mismatch for depth utilization.** Comparing a partially trainable model only
414 to full BP or to an unmatched random baseline can make weak methods look stronger than they are.
415 Diagnostic (d) uses architecture-matched frozen-blocks controls precisely so that “the deep blocks
416 helped” is tested against the right null.

417 **Pitfall 5: Silent train/eval mode inconsistencies.** Small mode mismatches can change residual
418 scale, normalization behavior, and therefore the diagnostic measurements themselves. The measure-
419 ment scripts fix model mode explicitly and log it, because otherwise a paper can end up comparing
420 training-time FA credit with evaluation-time BP references.

421 **Pitfall 6: Post-hoc normalization that erases scale pathology.** Renormalizing hidden states or
422 gradients before logging can make a genuine activation-growth failure disappear from the report. For
423 this paper, raw norms are part of the scientific object, so any normalization used for visualization
424 must remain separate from the values used for diagnosis.

425 **Pitfall 7: Missing null controls for intervention claims.** A rescue intervention can improve co-
426 sine or accuracy for trivial reasons unless the experiment includes a null such as fresh- B feedback
427 or a matched BP+penalty control. The paper therefore treats intervention evidence as incomplete
428 unless it separates training-specific adaptation from generic regularization or capacity effects [8–10].

429 C Walk-Back Chain Methodology

430 The walk-back chain is the compressed narrative used to translate a superficially positive headline
431 result into a falsifiable diagnostic verdict. It has four steps. Step 1 asks what the status-quo claim
432 would be from accuracy and headline Γ alone. Step 2 checks whether the deepest hidden-layer BP
433 reference remains numerically meaningful; if not, the alignment claim is walked back as ungrounded
434 measurement. Step 3 asks whether trained deep blocks outperform architecture-matched random-
435 block baselines; if not, the training claim is walked back as unused or weakly used depth. Step 4 uses
436 temporal replay, intervention, and cross-architecture evidence to determine whether the underlying
437 problem is primarily measurement degeneracy, low intrinsic credit-direction quality, or both.

438 This chain is deliberately asymmetric. A method can pass all four steps and remain provisionally
439 trustworthy, but failing any one of the binary detectors is enough to invalidate the stronger claim
440 that “deep local credit assignment is working” on that setting. That asymmetry matches the paper’s
441 goal: not to certify methods as universally good, but to prevent unsupported success claims from
442 surviving because the reporting pipeline asked too little of the evidence.

443 D All Seven Validations

444 Table 4 lists the seven validation exercises that support the protocol. They serve different purposes:
445 some validate binary detection, some validate interpretation, and some validate external usefulness.
446 Together they show that the protocol is not merely a post-hoc description of one final ResMLP
447 run, but a portable evaluation procedure that changes conclusions across time, interventions, and
448 architectures.

449 A useful way to read the table is that no single validation carries the paper by itself. The five-
450 method audit shows that the problem exists, temporal replay shows that the protocol is actionable,

Table 4: Summary of the seven validation exercises used to justify the protocol.

Validation	Question	Main observation	Why it matters
Five-method audit	Does the status quo over-credit methods?	Accuracy+ Γ walks back none; protocol walks back three	Establishes core decision gap
Decision-utility ablation	Which diagnostics are actually needed?	The full four-diagnostic stack is the first to separate controls from failures	Justifies protocol complexity
Temporal replay	Does the protocol fire early?	The detectors activate before final convergence	Makes the tool experimentally useful
Early-epoch DFA	Can mode 2 appear without mode 1?	Deep credit quality is poor while BP remains measurable	Separates the two modes
Penalty intervention	Can mode 1 be alleviated without full rescue?	Measurability improves more than deep credit quality	Shows intervention-specific response
Fresh- B and BP+penalty controls	Are rescue effects training-specific?	Some gains are generic, some remain method-specific	Prevents overclaiming intervention success
Cross-architecture audit	Which diagnostics generalize?	Activation growth generalizes more broadly than gradient-floor collapse	Scopes the claims correctly

451 intervention and null controls show that the two modes respond differently, and cross-architecture
 452 evidence shows which parts of the protocol are specific to terminal-normalized residual settings and
 453 which parts are more general.

454 E Threshold Sensitivity Full Sweep

455 The sensitivity sweep is intentionally small because the paper does not claim that all four thresholds
 456 are equally canonical. The important result is qualitative stability for diagnostics (a) and (b): over a
 457 reasonable range of nearby cutoffs, the same methods are flagged on the same audited settings, and
 458 the same controls remain unflagged. This is the strongest calibration evidence in the paper because
 459 these two diagnostics track the physical quantities most directly tied to the measurement-degeneracy
 460 story.

461 Diagnostic (d) is weaker and should be presented that way. Its threshold is best understood as
 462 a conservative reporting aid for depth utilization rather than as a universal constant. In practice,
 463 the full sweep should therefore be read as showing that the protocol is robust where it claims binary
 464 detection strength and intentionally modest where it is used as a contextual check on whether trained
 465 deep blocks beat architecture-matched random-block baselines.

466 F Per-Architecture Detailed Audits

467 The per-architecture appendix should be short and comparative. On pre-LayerNorm ResMLP and
 468 ViT-Mini, the key pattern is the same as in the main text: residual-scale growth can become large
 469 enough that the deepest BP reference becomes numerically weak, and the status-quo pair of accuracy
 470 plus headline Γ fails to expose that. These are the settings where both failure modes matter and
 471 where the full protocol is most necessary.

472 StudentNet and the CNN serve a different role. They test whether the protocol overgeneralizes from
 473 terminal-normalized residual architectures to settings where gradient-floor collapse is not expected.
 474 In those models, activation-growth checks can still reveal weak depth usage or poor scaling, but
 475 diagnostic (b) is not expected to fire in the same way. This asymmetry is not a weakness of the pro-
 476 tocol; it is part of the empirical scoping claim of the paper and helps prevent readers from mistaking
 477 a targeted evaluation standard for a universal pathology claim [12, 8].

478 **G Depth-Sweep Layerwise Profiles**

479 To check whether the layerwise pattern in Figure 1 is an artifact of the specific four-block depth
 480 used in the main audit, we ran the same architecture on $d=512$ pre-LayerNorm ResMLPs at five
 481 depths $L \in \{2, 4, 6, 8, 12\}$ on CIFAR-10 (single seed 42, otherwise matched configuration). Table 5
 482 reports the layer-0 cosine, the mean cosine over all deeper layers, and the deep mean perturbation
 483 correlation ρ for each depth.

Table 5: Depth sweep on $d=512$ ResMLP, seed 42, 100 epochs CIFAR-10. *layer-0 cos* is the embedding-block BP cosine, *deep cos* is the mean BP cosine over the remaining $L-1$ blocks, and *deep ρ* is the corresponding mean perturbation correlation. DFA’s deep credit signal is essentially zero at every depth, even though BP retains a deep cosine of $+0.94$ at $L=12$.

L	method	test acc	layer-0 cos	deep cos	deep ρ
2	BP	0.599	+1.000	+1.000	+0.983
2	DFA	0.312	+0.396	-0.005	+0.000
2	Credit Bridge	0.310	+0.330	+0.020	+0.000
4	BP	0.603	+1.000	+1.000	+0.988
4	DFA	0.314	+0.400	-0.000	+0.000
4	Credit Bridge	0.298	+0.402	+0.030	+0.000
6	BP	0.602	+0.993	+0.993	+0.991
6	DFA	0.310	+0.387	-0.000	+0.000
6	Credit Bridge	0.299	+0.304	+0.054	+0.000
8	BP	0.589	+0.965	+0.965	+0.992
8	DFA	0.306	+0.377	-0.000	+0.000
8	Credit Bridge	0.288	+0.205	+0.022	+0.000
12	BP	0.594	+0.942	+0.940	+0.990
12	DFA	0.309	+0.388	-0.000	+0.000
12	Credit Bridge	0.239	+0.208	+0.016	+0.000

484 The layerwise pattern is essentially depth-invariant. DFA’s layer-0 cosine stays in $[+0.39, +0.40]$
 485 across all five depths, while its mean deep cosine sits within $[-0.005, +0.000]$ and its deep ρ col-
 486 lapses to numerical zero in every condition. Credit Bridge shows a slightly milder version of the
 487 same shape, with a small positive deep cosine that does not improve as depth shrinks. BP, by
 488 contrast, maintains a deep cosine of $+0.94$ even at $L=12$, so the BP reference is still measurably
 489 non-degenerate where DFA and Credit Bridge are flat. The $L=4$ row, which matches the main au-
 490 dit’s architecture, has also been replicated across three seeds (42, 123, 456): 3-seed DFA layer-0
 491 cosine is $+0.412 \pm 0.011$, 3-seed DFA deep cosine is -0.0004 ± 0.0008 , and 3-seed CB deep cosine
 492 is $+0.039 \pm 0.010$, all statistically indistinguishable from the single-seed row shown in the table.
 493 This rules out the explanation that DFA’s deep blocks are merely too far from the loss to receive
 494 useful credit: making the network shallower does not reach the deep blocks any better. The failure
 495 is structural to the credit signal rather than an artifact of depth.

496 **H No-Residual Ablation: Skip Path Is Not the Proximate Trigger**

497 To test whether Mode 1 is specifically a property of the additive residual skip $h_{l+1} = h_l + F_l(h_l)$, we
 498 ran a matched ablation on the same 4-block $d=256$ ResMLP, on CIFAR-10, with the same optimizer,
 499 learning rate, weight decay, batch size, and seed (42), but replaced each block by $h_{l+1} = F_l(h_l)$ and
 500 increased the inner w_2 initialization standard deviation from 0.01 to 0.5 to make the no-residual
 501 stack trainable from step zero. Terminal LayerNorm and the rest of the architecture are unchanged.
 502 Three-epoch smoke results:

503 The qualitative shape matches what we see in vanilla residual DFA, only with a slower onset because
 504 the architecture itself is harder to train. Diagnostic (a) clearly fires within three epochs, and diag-
 505 nostic (b) is already on the floor side of 10^{-7} . Across w_2 std values $\{0.1, 0.2, 0.5\}$ that we tried in
 506 the same smoke sweep, the qualitative outcome is the same: residual stream grows by three to four
 507 orders of magnitude, $\|g_L\|$ drops by three to four orders of magnitude, and BP itself never reaches a
 508 healthy training regime. We retain $w_2=0.5$ here because that is the only value where BP is at least
 509 beginning to learn. The full 100-epoch trajectory of the same configuration, replicated across three

Table 6: No-residual ResMLP-d256 ablation, seed 42, 3 epochs each. Without the additive skip path, DFA’s residual stream still grows several orders of magnitude in three epochs and the deepest BP reference still trends toward the gradient floor, so the residual skip is not necessary for Mode 1. BP also struggles in this regime (the architecture is partially degenerate), which limits the strength of the algorithm comparison but does not change the necessity claim for Mode 1.

method	w_2 std	ep	$\ h_L\ $	$\ g_L\ $	test acc	gamma_dfa
BP	0.5	0	4.69	9.8×10^{-4}	0.080	—
BP	0.5	1	155	4.3×10^{-5}	0.144	—
BP	0.5	2	174	4.0×10^{-5}	0.164	—
BP	0.5	3	163	4.2×10^{-5}	0.163	—
DFA	0.5	0	4.69	9.8×10^{-4}	0.080	—
DFA	0.5	1	5,295	8.6×10^{-7}	0.156	0.047
DFA	0.5	2	16,930	2.2×10^{-7}	0.151	0.040
DFA	0.5	3	22,050	1.6×10^{-7}	0.148	0.039

510 seeds (42, 123, 456), converges to a mean $\|h_L\| \approx 8.2 \times 10^7$ and mean $\|g_L\| \approx 1.9 \times 10^{-10}$ (per-
511 seed values $\|h_L\| \in \{1.06 \times 10^8, 3.15 \times 10^7, 1.09 \times 10^8\}$ and $\|g_L\| \in \{1.08, 2.94, 1.77\} \times 10^{-10}$),
512 all deeply below the diagnostic (b) floor and within an order of magnitude of vanilla residual DFA’s
513 $\|h_L\| \approx 4 \times 10^8$ and $\|g_L\| \approx 5 \times 10^{-10}$ on the same backbone, confirming that the smoke-test trend
514 is the converged behavior rather than an early-training artifact.

515 We treat this ablation as evidence about *necessity*, not about clean algorithm separation. Specifically,
516 the evidence supports: the additive residual skip is not necessary for Mode 1 activation growth
517 or for the gradient-floor trend; Mode 1 (a) appears to be a generic deep-DFA instability on these
518 stacks, modulated but not gated by skip presence; and the catastrophic, well-defined $\|g_L\|$ collapse
519 remains most tightly associated with terminal LayerNorm in our audited settings, where the no-
520 out_ln control already showed activation growth without the same severity of collapse. The full
521 100-epoch trajectory of this no-residual run is reported as a confirmatory check rather than as a
522 primary claim.

523 I Random-Target Ablation: Mode 1 Is Data-Agnostic

524 To test whether Mode 1 activation growth requires any task signal at all, we re-ran DFA on the stan-
525 dard 4-block $d=256$ pre-LayerNorm ResMLP, on CIFAR-10 inputs, but replaced each minibatch’s
526 labels with i.i.d. random class targets drawn fresh from a uniform distribution over $\{0, \dots, 9\}$. All
527 other hyperparameters are matched to the vanilla DFA training run in Section 2 (AdamW, lr= 10^{-3} ,
528 wd= 0.01, 128 batch, cosine schedule, single seed 42 for the smoke test). The local feedback vectors
529 B_l are unchanged. Three-epoch trajectory:

Table 7: Random-target ablation, DFA on the standard residual ResMLP-d256, seed 42, three epochs of training with i.i.d. random class targets refreshed every minibatch. The network does not learn anything (test accuracy stays near chance), yet $\|h_L\|$ grows three orders of magnitude and $\|g_L\|$ drops three orders of magnitude in the same three epochs, matching the qualitative trajectory of the real-label DFA run on the same backbone.

ep	$\ h_L\ $	$\ g_L\ $	test acc	gamma_dfa
0	8.89	9.83×10^{-4}	0.115	—
1	1,616	5.12×10^{-6}	0.078	-0.020
2	9,768	8.50×10^{-7}	0.081	-0.024
3	14,510	5.62×10^{-7}	0.071	-0.025

530 This ablation answers the natural counterargument that DFA’s residual-stream growth might be a
531 side-effect of the network adapting to genuine task signal in a particularly bad local minimum: it
532 is not. With no task signal at all, DFA on this architecture still inflates the residual stream by more
533 than three orders of magnitude in the first three epochs and pushes the deepest BP reference gradient
534 to the floor of 10^{-7} in the same window. The full 100-epoch trajectory of the same DFA random-
535 target run converges to $\|h_L\| \approx 1.67 \times 10^8$ and $\|g_L\| \approx 8.0 \times 10^{-12}$, both more extreme than

536 the corresponding endpoints of vanilla DFA on the same backbone with real labels (about 4×10^8
537 and 5×10^{-10} respectively), so the data-agnostic trajectory does not just reach Mode 1 but in fact
538 passes through the same regime even without any per-sample task pressure. The local DFA objective
539 $\langle f_i(h_i), e_T B_i^T \rangle$ contains no penalty on $\|f_i(h_i)\|$, so any direction in which a larger block output
540 increases inner-product alignment with the fixed feedback target is rewarded; the random-target run
541 isolates exactly this geometric incentive, free of any task-driven feature pressure. The full 100-epoch
542 trajectory of this random-target run is reported as a confirmatory check rather than a primary claim.

543 We then asked whether this data-agnostic growth is specific to DFA or generalizes to other fixed-
544 feedback local-credit methods, by repeating the random-target ablation under State Bridge and
545 Credit Bridge with the same architecture, hyperparameters, and seed. Both methods also exhibit
546 data-agnostic activation growth in the same three-epoch window, with $\|h_L\|$ rising from about 9 to
547 about 6.2×10^3 (State Bridge) and about 2.0×10^4 (Credit Bridge), while their test accuracies remain
548 at chance (0.10 and 0.09, respectively):

Table 8: Random-target ablation across the three audited fixed-feedback local-credit methods on the standard residual ResMLP-d256, seed 42, three epochs of training with i.i.d. random class targets. All three methods show data-agnostic $\|h_L\|$ growth even though no task signal is being learned. SB and CB grow more slowly than DFA in absolute magnitude, consistent with their bridge-style normalization providing partial scale damping but not preventing growth.

method	$\ h_L\ $ at ep 3	$\ g_L\ $ at ep 3	test acc
DFA	14,510	5.6×10^{-7}	0.071
State Bridge	6,225	1.0×10^{-5}	0.104
Credit Bridge	19,974	3.2×10^{-6}	0.092

549 The cross-method version of the test rules out the explanation that the random-target growth is
550 specific to DFA’s particular feedback projection. State Bridge and Credit Bridge use bridge con-
551 structions with target normalization and stop-gradients, so any residual-stream growth they exhibit
552 cannot be attributed to a simple absence of normalization. Their $\|g_L\|$ values at three epochs are
553 still well above the 10^{-7} floor used by diagnostic (b), so the gradient collapse part of Mode 1 does
554 not yet appear at this horizon for SB/CB; the activation-growth part of Mode 1 is already present.
555 At the full 100-epoch trajectory of the same random-target protocol, both SB and CB also reach
556 the (b) floor: SB converges to $\|h_L\| \approx 3.6 \times 10^5$ and $\|g_L\| \approx 4 \times 10^{-8}$, and CB converges to
557 $\|h_L\| \approx 1.38 \times 10^8$ and $\|g_L\| \approx 0$ (below the numerical clamp), with test accuracies 0.100 and
558 0.085 respectively, consistent with DFA’s 1.67×10^8 and 8.0×10^{-12} at the same horizon. We
559 treat this as evidence that the local-credit growth incentive is not unique to DFA but is shared by the
560 audited family of fixed-feedback methods.

561 The cleanest negative control for the random-target assay is Equilibrium Propagation, which trains
562 the same backbone with a contrastive nudged-vs-free local energy objective rather than a fixed feed-
563 back projection. We re-ran EP on the same ResMLP-d256 with i.i.d. random class targets, seed 42,
564 identical hyperparameters: EP’s $\|h_L\|$ stays at about 586 at five epochs of training and converges to
565 about 2,085 over the full 100-epoch trajectory, which is roughly $25\times$ smaller than DFA’s 14,510 at
566 three epochs and is in the same range as vanilla EP’s bounded trajectory on real labels ($\sim 5 \times 10^3$).
567 At convergence, the random-target EP run reaches headline accuracy 0.081, headline $\Gamma = -0.0003$,
568 and headline $\rho = -0.006$, all consistent with chance-level performance and a non-degenerate mea-
569 surement regime. The random-target assay therefore separates the audited fixed-feedback methods
570 (DFA/SB/CB) from EP cleanly: fixed-feedback objectives without an explicit scale-control term ex-
571 hibit data-agnostic activation growth on this architecture, while EP’s energy-based local objective
572 does not.

573 J State Bridge Penalty Rescue: 3-Seed Cross-Method Test

574 To test whether the per-block scale-control penalty $\lambda \text{mean}(\|f_i(h_i)\|^2)$ that rescues DFA in Sec-
575 tion 5 also rescues other audited fixed-feedback local-credit methods, we re-ran State Bridge on
576 the standard 4-block $d=256$ pre-LayerNorm ResMLP for 30 epochs and three seeds (42, 123, 456),
577 with $\lambda=10^{-2}$ added to the State Bridge per-block local loss only (the bridge state predictor and the
578 embedding/head paths are not penalized, matching the DFA rescue setup). We also ran a matched

579 vanilla State Bridge baseline at seed 42 with the same architecture and training schedule but $\lambda=0$.
 580 Three-seed converged values:

Table 9: State Bridge with the same per-block scale-control penalty $\lambda=10^{-2}$ that rescues DFA in Section 5, on the 4-block $d=256$ pre-LayerNorm ResMLP, 30 epochs, three seeds. SB+penalty reaches a converged test accuracy of 0.453 ± 0.003 , exceeding the architecture-matched frozen-blocks shallow baseline of 0.349 by +10.4 percentage points and the DFA+penalty value of 0.363 ± 0.001 by +9.0 percentage points. The deep mean cosine and deep mean perturbation correlation are roughly $2\times$ and $5\times$ the corresponding DFA+penalty values respectively, while the residual stream is contained but not silenced ($\|h_L\| \approx 302$, $\|g_L\| \approx 1.8 \times 10^{-4}$). Vanilla SB on the same architecture and seed reaches only 0.213, with $\|h_L\| \approx 9.85 \times 10^6$ and $\|g_L\|$ at the diagnostic-(b) floor.

seed	test acc	$\ h_L\ $	$\ g_L\ $	deep cos	deep ρ
SB+pen 42	0.4564	302	1.75×10^{-4}	+0.312	+0.392
SB+pen 123	0.4514	311	1.74×10^{-4}	+0.327	+0.424
SB+pen 456	0.4509	292	1.92×10^{-4}	+0.326	+0.391
SB+pen mean	0.453 ± 0.003	302 ± 8	1.80×10^{-4}	$+0.322 \pm 0.007$	$+0.402 \pm 0.015$
CB+pen 42	0.3596	5431	1.88×10^{-5}	+0.684	+0.498
CB+pen 123	0.3642	5834	1.81×10^{-5}	+0.667	+0.452
CB+pen 456	0.3562	5775	2.01×10^{-5}	+0.685	+0.442
CB+pen mean	0.360 ± 0.003	5680 ± 178	1.90×10^{-5}	$+0.679 \pm 0.008$	$+0.464 \pm 0.025$
vanilla SB 42	0.213	9.85×10^6	1×10^{-8}	—	—
vanilla CB 42	0.211	6.7×10^7	~ 0	—	—
DFA+pen mean (3 seeds)	0.363 ± 0.001	4.0×10^4	9.0×10^{-7}	$+0.155 \pm 0.025$	$+0.080 \pm 0.011$

581 The penalty rescue effect on State Bridge is much larger than on DFA: +24 percentage points for
 582 State Bridge versus +5.5 percentage points for DFA on the same architecture and intervention.
 583 SB+penalty is the first audited non-BP method whose trained deep blocks substantively beat the
 584 architecture-matched random-block baseline. We treat this as evidence that Mode 2 (low intrinsic
 585 credit-direction quality) has method-dependent severity within the audited fixed-feedback family
 586 once Mode 1 is alleviated, rather than being a uniform property of all fixed-feedback local-credit ob-
 587 jectives. Importantly, State Bridge’s deep cosine +0.322 is approximately twice DFA’s +0.155 on
 588 the same intervention, but neither approaches the BP reference value of $\approx +1.0$, so this is a within-
 589 class gradation in credit-direction quality, not a claim that bridge constructions “solve” Mode 2.
 590 Under the same intervention Credit Bridge reaches a three-seed test accuracy of 0.360 ± 0.003 , a
 591 three-seed deep mean cosine of $+0.679 \pm 0.008$, and a three-seed deep mean ρ of $+0.464 \pm 0.025$,
 592 with $\|h_L\| \approx 5680 \pm 178$ and $\|g_L\| \approx 1.9 \times 10^{-5}$ well above the diagnostic floor. Credit Bridge
 593 therefore has an even higher deep cosine than State Bridge (about $4\times$ the DFA value and roughly
 594 $2\times$ the State Bridge value), but reaches the same final accuracy as DFA+penalty and 9.3 percentage
 595 points below State Bridge+penalty. This is a clean dissociation: within the audited fixed-feedback
 596 family under the same rescue, deep cosine and deep ρ differ by more than a factor of four across
 597 methods without tracking final accuracy in the same direction, so alignment to the BP gradient is
 598 a necessary but not sufficient diagnostic of usable credit for depth. That cross-method dissociation
 599 is a direct reason the protocol in Section 6 keeps final accuracy, layerwise credit quality, and the
 600 depth-utilization baseline as three separate reporting axes rather than collapsing them into a single
 601 headline.

602 K Reproducibility

603 All headline audit results in the main text should be reported over the locked seed set $\{42, 123, 456\}$,
 604 with the same seed bundle reused across methods wherever possible so that between-method com-
 605 parisons are not driven by different data orders or initialization luck. Every released result table
 606 should specify the architecture, optimizer, learning-rate schedule, batch size, augmentation recipe,
 607 number of epochs, checkpoint selection rule, and whether each diagnostic was measured at the final
 608 checkpoint or along a stored temporal trajectory.

609 Hyperparameters should be listed exactly as run, not reconstructed from memory after the fact. For
 610 intervention experiments, the appendix should report the penalty coefficient, where in the network

611 the penalty is applied, and which control runs share the same added objective. For diagnostic scripts,
612 reproducibility requires logging the model mode, minibatch identity, and layer-index convention
613 used for per-layer statistics. The point of this appendix is simple: because the paper's claims hinge
614 on how evaluation is performed, measurement configuration is part of the result and must be repro-
615 ducible with the same care as training configuration.